Available online at www.sciencedirect.com
SCIENCE DIRECT®
PERGAMON
International Journal of Heat and Mass Transfer 46 (2003) 4717–4732
International Journal of HEAT and MASS TRANSFER
www.elsevier.com/locate/ijhmt

Interaction of a moving shock wave with a two-phase reacting medium

Jun Sung Park, Seung Wook Baek *

Division of Aerospace Engineering, Department of Mechanical Engineering, Korea Advanced Institute of Science and Technology, 373-1 Kusung-Dong, Yusong-Gu, Taejon 305-701, South Korea

Received 19 December 2002

Abstract

The flow field, that develops when a moving shock wave hits a two-phase medium of gas and particles, has a practical application to industrial accidents such as explosions at coal mine and in grain elevator and furthermore to solid propellant combustion in rocket engine. Therefore, a successful prediction of the thermo-fluid mechanical characteristics development of gas and particles is very crucial and imperative for the successful design and operation of rocket nozzles and energy conversion systems. This paper describes an interaction phenomenon when a moving shock wave hits a two-phase medium of gas and particles with/without chemical reaction. A particle-laden gas is considered to be located along a ramp so that numerical integration is accomplished from the tip of ramp for a finite period. For the numerical solution, a fully conservative unsteady implicit second order time-accurate sub-iteration method and the second order Total Variation Diminishing scheme are used with the finite volume method for gas phase. For particle phase, the Monotonic Upstream Schemes for Conservation Laws as well as the solution of the Riemann problem for the particle motion equations is also used together with the schemes above. Transient development of thermo-fluid mechanical characteristics is calculated and discussed by changing the particle mass density and particle specific heat. For the case of the reacting particle-laden gas flow, a carbon particle-laden oxygen gas is considered to be located along a ramp. The results are discussed by comparison with the cases of the pure gas and the inert particle-laden gas. Major results reveal that when the particle mass density is smaller, there is a stronger interaction between two phases so that the velocity and temperature differences between two phases more rapidly decrease. When the particle specific heat is varied, only a thermal effect is observed while the other effects are minor. The case with reacting particles yields significantly different results due to chemical reaction such that the gas density does not monotonously but rapidly decrease due to the slip line in the relaxation zone, while the pressure and temperature become higher in comparison with the non-reacting case. But the dynamic variation would be only secondary to the thermal one.

Keywords: Two phases compressible flow; Shock ignition; Shock wave diffraction; Particle and physical parameters; Compression corner

1. Introduction

The flow field, that develops when a moving shock wave hits a two-phase medium of gas and particles, has a close practical relation to industrial applications (e.g. solid rocket engine in which aluminum particles are used to reduce the vibration due to instability) as well as industrial accidents such as explosions in coalmines and grain elevators. In the above cases, non-reacting or reacting solid particles are involved in the gas phase.

There have been a few experimental as well as several analytical or numerical studies that examined two-phase medium effects on the gas flow field. Carrier [1] and Rudinger [2] proposed the general equations governing a shock wave interaction with two-phase medium of air

* Corresponding author. Tel.: +82-42-869-3714; fax: +82-42-869-3710.
E-mail address: swbaek@sorak.kaist.ac.kr (S.W. Baek).

0017-9310/$ - see front matter
doi:10.1016/S0017-9310(03)00310-7

Nomenclature

A, B, C	*Jacobian* matrices
a	speed of sound (m/s)
C_d	viscous drag coefficient
C_i	mass concentration (kg/m^3)
C_p, C_v	specific heat of gas at constant pressure and volume respectively (J/kg K)
C_{pp}	specific heat of particle (J/kg K)
E, F, H	flux vectors
e	internal energy of gas (J/kg)
e_t	total internal energy of gas (J/kg)
e_p	total internal energy of particle (J/kg)
D_p	particle diameter (μm)
f_p	viscous drag between gas and particles (N/m^3)
h	total enthalpy of gas (J/kg)
J	*Jacobian*, $\xi_x\eta_y - \eta_x\xi_y$
k	thermal conductivity of gas (J/m K s)
L	reference length (m)
M	Mach number
Nu	Nusselt number
P	gas mixture pressure (Pa)
Pr	Prandtl number
Q	conservative state vector
q_p	heat flux between gas and particles (W/m^2)
R	residual
Re	gas Reynolds number
Re_p	particle Reynolds number, $\rho D_p \Delta U/\mu$
R_u	universal gas constant (J/kmol K)
R_m	gas constant (J/kmol K)
S	source term
T	temperature (K)
t	time (s)
u, v	velocities (m/s)
ΔU	slip velocity, $\sqrt{(u-u_p)^2+(v-v_p)^2}$ (m/s)
x, y	Cartesian coordinates (m)
x_i	ith mole fraction
Y_i	ith mass fraction
W	molecular weight (kg/kmol)

Greek symbols

ξ, η	generalized curvilinear coordinates
ρ	gas density (kg/m^3)
ρ_p	particle concentration (kg/m^3)
μ	dynamic viscosity (kg/m s)
γ	specific heat ratio of gas (C_p/C_v)
λ	eigenvalues
σ_p	mass density of particle per unit volume (kg/m^3)
ϕ	mass fraction ratio of particles, $\rho_p/(\rho+\rho_p)$
θ_w	compression corner angle (°)

Superscripts

n	time index
$-$, $*$	non-dimensional quantities

Subscripts

i, j	space indices
C	carbon
ch	chemical reaction
m	mixture
o	at stagnation state or ahead of a moving shock
p	particle phase
r	reference state
s	shock
w	wall
∞	ambient state

and glass beads, and studied their thermo-fluid mechanical behaviors, based on a perfect gas assumption. A comprehensive review of gas–particle nozzle flows was presented by Hoglund [3]. This paper performed two-phase theoretical and experimental studies, and discussed about the one-dimensional approximation. A complete review of numerical models for dilute gas–particle flows has been presented by Crowe [4], who also categorized the models according to its type of coupling, dimension and approach. The advantages and disadvantages of two-fluid and trajectory models were also discussed therein. Since the 1970s, numerical methods have been broadly applied to a complicated set of governing equations. Chang [5] used the MacCormack Scheme to study the gas and particle flow patterns in axi-symmetric convergent–divergent nozzles (JPL nozzle, and Titan III and IUS solid rocket motors) by changing such parameters as particle diameter and particle mass fraction. Marconi et al. [6] used the characteristic(λ) method to analyze the one-dimensional unsteady particle-laden gas flow.

In 1980s, Elperin et al. [7] and Igra et al. [8] analyzed the interaction of a normal shock wave with carbon-particle laden oxygen gas. These papers investigated a variation of physical phenomena in relaxation zone, provided that the properties of carbon particles were constant during the reaction. Gokhale and Bose [9] extended a non-reacting two-phase flow to reacting one in one-dimensional nozzle by using the explicit MacCormack Scheme. Nishida and Ishimaru [10] have obtained the numerical solution for gas–solid two-phase non-equilibrium nozzle flows using the MacCormack's scheme with Total Variation Diminishing (TVD). More recently, Mehta and Jaychandran [11] proposed a fast

algorithm to solve viscous two-phase flow in an axisymmetric rocket nozzle, whereas Igra et al. [12] investigated two-phase flow in outside free stream region as well as inside nozzle. Bendor et al. [13] studied various reflection patterns of planar shock waves from straight wedges in dust–gas suspensions. The results provided a clear picture of whether and how the presence of dust particles affects the shock-reflection-induced flow field.

The purpose of this study is to describe interaction phenomena when a moving shock wave hits a two-phase medium of gas and particles considering the effects of particle combustion. To calculate the gas and particle flow developments, the governing equations with terms accounting for particle reaction are non-dimensionalized and accurate correlations regarding particle drag and heat transfer between gas and particles are used. The Eulerian type of equations are solved for the particles as well as the gas flow. For the numerical solution, a fully conservative unsteady implicit second order time accurate sub-iteration method [14] and a second order TVD scheme [15] are used with the finite volume method (FVM) for the gas phase. For the particle phase, Monotonic Upstream Schemes for Conservation Laws (MUSCL) [16] as well as the solution of the Riemann problem for the particle motion equations [17] is used. The results are discussed by comparison with those for the case of the pure gas flow. To author's best knowledge, so far there is no paper reporting the thermo-fluid mechanical properties of two-dimensional shock wave interaction with a reacting two-phase flow.

2. Governing equations

As schematized in Fig. 1, the current paper deals with a shock wave interaction with an inert particle-laden gas for the non-reacting case and a carbon particle-laden oxygen gas for the reacting case, when a two-dimensional 27° ramp exists in the flow passage. When a shock wave hits a two-phase medium, the gas phase velocity is instantly accelerated and its temperature rapidly increases. However, the particle velocity and temperature do not immediately respond to a physical change in gas because of the inertia and heat capacity of particles. These effects incur the velocity slip and temperature difference between the gas and particle phases, whereby the momentum and energy are transferred between them. Through these interactions, the gas and particle phases finally reach the equilibrium state in the long run. Since the rates of momentum and energy exchanges are quite limited within 100 μs during which the numerical simulation is done, the gas and the particles are still out of equilibrium. For the present analysis, the following assumptions are introduced.

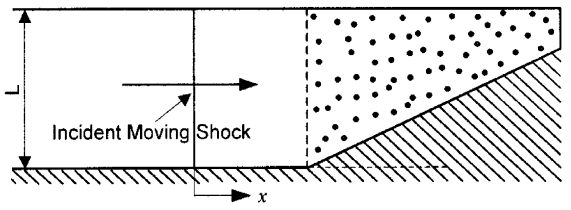

Fig. 1. A schematic of the particle-laden gas suspension with an incident shock wave.

1. The gas and particle flows are two-dimensional and continuous.
2. The particles are spherical and uniform in size at a given location.
3. The volume occupied by the particles is negligible while the particles do not interact with each other.
4. No temperature distribution occurs inside the particles.
5. There are viscous momentum transfer and heat transfer between gas and particles.
6. The effect of the radiative heat transfer is negligible.
7. The thermal and Brownian motions of the particles are negligible.
8. Before the shock wave interaction with the two-phase mixture, it is in a state of thermodynamic and kinematic equilibrium.

The governing equations for gas flow are the time-dependent compressible Euler equations in a strongly conservative form. For two-phase flow, the governing equations are written in the form of the Eulerian–Eulerian formulation. The unsteady conservation equations for the gas phase are in the following form:

$$\frac{\partial Q}{\partial t}+\frac{\partial E}{\partial x}+\frac{\partial F}{\partial y}+H_1=H_2, \tag{1}$$

where Q is the conservative flow variable vector and E and F are the inviscid flux vectors

$$Q=\begin{bmatrix}\rho\\ \rho u\\ \rho v\\ \rho e_t\\ \rho Y_i\end{bmatrix},\quad E=\begin{bmatrix}\rho u\\ \rho u^2+P\\ \rho uv\\ u(\rho e_t+P)\\ \rho uY_i\end{bmatrix},$$

$$F=\begin{bmatrix}\rho v\\ \rho uv\\ \rho v^2+P\\ v(\rho e_t+P)\\ \rho vY_i\end{bmatrix}.$$

The source terms H_1 and H_2 are denoted by

$$H_1 = \begin{bmatrix} 0 \\ f_{px} \\ f_{py} \\ q_p + u_p f_{px} + v_p f_{py} \\ 0 \end{bmatrix}, \quad H_2 = \begin{bmatrix} S \\ uS \\ vS \\ q_{ch} S \\ S_i \end{bmatrix}.$$

These terms represent momentum and heat exchanges between gas and particles, and the chemical reaction, respectively.

The governing equations for the particle phase are also cast in the following conservative form:

$$\frac{\partial Q_p}{\partial t} + \frac{\partial E_p}{\partial x} + \frac{\partial F_p}{\partial y} + H_{p1} = H_{p2}, \tag{2}$$

where

$$Q_p = \begin{bmatrix} \rho_p \\ \rho_p u_p \\ \rho_p v_p \\ \rho_p e_p \end{bmatrix}, \quad E_p = \begin{bmatrix} \rho_p u_p \\ \rho_p u_p^2 \\ \rho_p u_p v_p \\ \rho_p u_p e_p \end{bmatrix}, \quad F_p = \begin{bmatrix} \rho_p v_p \\ \rho_p u_p v_p \\ \rho_p v_p^2 \\ \rho_p v_p e_p \end{bmatrix},$$

$$H_{p1} = \begin{bmatrix} 0 \\ -f_{px} \\ -f_{py} \\ -q_p - u_p f_{px} - v_p f_{py} \end{bmatrix}, \quad H_{p2} = \begin{bmatrix} S_p \\ u_p S_p \\ v_p S_p \\ q_{ch,p} S_p \end{bmatrix}.$$

Since the volume occupied by the particles is negligible, the viscous drag between gas and particles is dominant so that the momentum exchange terms for particles of spherical shape [18] can be denoted by

$$f_{px} = \frac{3}{4} \frac{\rho_p \rho}{D_p \sigma_p} C_d (u - u_p) \Delta U, \tag{3}$$

$$f_{py} = \frac{3}{4} \frac{\rho_p \rho}{D_p \sigma_p} C_d (v - v_p) \Delta U, \tag{4}$$

where C_d is the drag coefficient and ΔU is slip velocity, which is defined as $\Delta U = \sqrt{(u-u_p)^2 + (v-v_p)^2}$. The energy transfer rate between gas and particles [18] is

$$q_p = \frac{\mu}{Re_\infty Pr(\gamma - 1)} 6Nu \frac{\rho_p}{D_p^2 \sigma_p} (T - T_p). \tag{5}$$

In the above equations, all variables are non-dimensionalized using reference flow and physical properties such as L, ρ_∞, T_∞, a_∞, μ_∞. And three non-dimensionalized parameters appear in the governing equations as follows:

$$Re_\infty = \frac{\rho_\infty a_\infty L}{\mu_\infty}, \quad M = \frac{u}{a}, \quad Pr = \frac{\mu C_p}{k}.$$

The drag coefficient and Nusselt number used here are the ones proposed by Cliff et al. [19]. They are respectively corrected following Henderson [20] and Carlson and Hoglund [21] which take account of the rarefaction effect of gas and the supersonic effect by using a relative Mach number.

For a calculation of reacting flows, the evaluation of thermo-physical properties is of vital importance. In this paper, the specific heat C_p and thermal conductivity k for each species are determined by third order polynomials of temperature, and the viscosity μ is evaluated using the Sutherland formula for each species

$$\mu = \mu_0 \left(\frac{T}{T_0} \right)^{3/2} \frac{T_0 + S_0}{T + S_0}, \tag{6}$$

where S_0 is the constant for Sutherland's law.

The thermo-physical properties of the mixture are calculated using Wilke's mixing rule. While the temperature is implicitly determined using the definition of internal energy

$$e_i = \int_{T_{ref}}^{T} C_{pi} \, dT + h_{fi}^0 - \frac{R_u T}{W_i}, \tag{7}$$

the pressure P is then determined from the equation of state for a mixture of gases

$$P = \rho R_u T \sum_{i=1}^{NS} \frac{Y_i}{W_i}, \tag{8}$$

where NS represents the number of chemical species involved in chemical reactions.

Additionally, the carbon burning rate needs to be determined for the reacting case. In this work, the carbon reaction takes place in a pure oxygen environment. Furthermore, the initial amount of carbon is much smaller than that of oxygen so that it is reasonable to assume that the carbon is fully oxidized to carbon dioxide. Therefore, the following single step chemical reaction model is used here to describe the carbon reaction rate:

$$C(s) + O_2(g) \rightarrow CO_2(g) + 3.937 \times 10^5 \text{ kJ/kmol}. \tag{9}$$

Considering the above chemical reaction, the components of chemical reaction source vector are composed as follows.

$$q_{ch} = \frac{C_{pp}}{\gamma R} T_p + \frac{h_b}{a_\infty^2}, \tag{10}$$

$$S = -S_p = \frac{W_C \rho_C r_C}{m_C} \times \frac{L}{a_\infty}, \tag{11}$$

$$q_{ch,p} = \frac{C_{pp}}{\gamma R} T_p, \tag{12}$$

where h_b is the heat of formation of CO_2 and r_C is the carbon burning rate, which is represented by Baek and Seung [22] such that

$$r_C = \pi D_p^2 k_C C_{O_2} \text{ (kmol/s)}, \tag{13}$$

$$k_C = \frac{R_u T_m / W_C}{1/k_s + 1/k_d}, \tag{14}$$

$$k_s = 0.86\exp(-1.4947\times 10^8/R_u T_p), \tag{15}$$

$$k_d = 2.43\times 10^{-2}\phi D_d/D_p R_m T_m, \tag{16}$$

where D_d, C_{O_2} and T_m are the molecular diffusivity, the oxygen mass fraction and the arithmetic average of temperature, respectively.

3. Numerical methods

Eqs. (1) and (2) constitute the hyperbolic type of equations, of which each variable is closely coupled with the others. There exist a lot of numerical methods for solving this type of systems. In the present analysis, the FVM is employed since this method is known to easily satisfy the conservation rules and to be computationally stable at the surface of discontinuities. First of all, a physical space is transformed to a computational space in order to promote the numerical efficiency and conveniently apply the physical boundary conditions using the following coordinate transformation.

$$\xi = \xi(x,y), \tag{17}$$

$$\eta = \eta(x,y). \tag{18}$$

After the coordinate transformation, Eqs. (1) and (2) become

$$\frac{\partial \overline{Q}}{\partial t} + \frac{\partial \overline{E}}{\partial \xi} + \frac{\partial \overline{F}}{\partial \eta} + \overline{H}_1 = \overline{H}_2, \tag{19}$$

$$\frac{\partial \overline{Q}_p}{\partial t} + \frac{\partial \overline{E}_p}{\partial \xi} + \frac{\partial \overline{F}_p}{\partial \eta} + \overline{H}_{p1} = \overline{H}_{p2}, \tag{20}$$

where

$$\overline{Q} = \frac{1}{J}Q, \quad \overline{E} = \frac{1}{J}(\xi_x E + \xi_y F),$$

$$\overline{F} = \frac{1}{J}(\eta_x E + \eta_y F), \quad \overline{H}_1 = \frac{1}{J}H_1, \quad \overline{H}_2 = \frac{1}{J}H_2,$$

$$\overline{Q}_p = \frac{1}{J}Q_p, \quad \overline{E}_p = \frac{1}{J}(\xi_x E_p + \xi_y F_p),$$

$$\overline{F}_p = \frac{1}{J}(\eta_x E_p + \eta_y F_p), \quad \overline{H}_{p1} = \frac{1}{J}H_{p1}, \quad \overline{H}_{p2} = \frac{1}{J}H_{p2}.$$

Jacobian, J represents the volume of each cell in the Cartersian coordinate system.

3.1. Gas phase

In order to solve the gas phase equations (19), the second order TVD scheme and Roe's average are used together with the FVM, thereby improving the resolution of discontinuities in a reacting compressible flow. For TVD scheme, the limiter employed is a less compressive van Leer limiter for nonlinear fields, while a more compressive superbee limiter for the linear fields.

3.2. Particle phase

Contrary to the gas phase, the particle properties do not abruptly change across a shock wave. But the particles are only located from the position of the slanted wall so that there is some region where none of particles exist as seen in Fig. 1. To deal with this problem, the particle phase equations (20) are to be solved in a similar manner to the gas phase. Now, the MUSCL with minmod limiter as well as the solution of the Riemann problem for the particle motion equations [17] is applied.

3.3. Time splitting method

To solve the equations involved with the conservative vector variables, the LU decomposition proposed by Jameson and Turkel [23] is used. It has the advantage to reduce the computational efforts in calculating the inverse matrices. In this analysis, the implicit second order time accurate sub-iteration method [14] is also employed to obtain the following more precise unsteady solution:

$$\begin{aligned}\Delta\overline{Q}^n &= \frac{2\Delta t}{3}\frac{\partial}{\partial t}(\Delta\overline{Q}^n) + \frac{2\Delta t}{3}\frac{\partial}{\partial t}\overline{Q}^n + \frac{1}{3}\Delta\overline{Q}^{n-1}\\ &= \frac{2\Delta t}{3}\left(\frac{\partial}{\partial t}\overline{Q}^{n+1} - \frac{\partial}{\partial t}\overline{Q}^n\right) + \frac{2\Delta t}{3}\frac{\partial}{\partial t}\overline{Q}^n + \frac{1}{3}\Delta\overline{Q}^{n-1}\\ &= \frac{2\Delta t}{3}\left(-\frac{\partial \overline{E}^{n+1}}{\partial \xi} - \frac{\partial \overline{F}^{n+1}}{\partial \eta} - \overline{H}_1^{n+1} + \overline{H}_2^{n+1}\right)\\ &\quad + \frac{1}{3}\Delta\overline{Q}^{n-1},\end{aligned} \tag{21}$$

$$\begin{aligned}&\Delta\overline{Q}^p + \frac{2\Delta t}{3}\left(\frac{\partial \overline{E}^{p+1}}{\partial \xi} + \frac{\partial \overline{F}^{p+1}}{\partial \eta} + \overline{H}_1^{p+1} - \overline{H}_2^{p+1}\right)\\ &\quad = -(\overline{Q}^p - \overline{Q}^n) + \frac{1}{3}\Delta\overline{Q}^{n-1}.\end{aligned} \tag{22}$$

4. Initial and boundary conditions

In this analysis of the unsteady two-phase flow over a ramp, the gas and the particles are initially supposed to be in thermal equilibrium and at rest. Also are they uniformly distributed along a ramp as shown in Fig. 1.

At upper and lower walls, a slip as well as adiabatic condition is imposed since the flow is assumed to be inviscid and impermeable. At the outlet, the outflow condition of the first order extrapolation is used, because an incident shock wave moves at the supersonic speed, while at the inlet the boundary conditions for gas

are determined by the post conditions after the given shock wave by equating the Fanno line equation and the Rayleigh line equation.

For the particle phase, the different conditions are applied. At the walls, the slip condition (neither adherence nor reflection condition) as well as the impermeable condition is provided, and other properties are extrapolated from the inner ones. The inlet and outlet boundary conditions are initially given such that there are no particles at the inlet. The numerical computation is finished before the shock wave front reaches the outlet of the domain.

In this problem, initially the mixture is assumed to be at rest and in a state of thermodynamic and kinematic equilibrium before shock wave interaction. Under the above conditions, the physical domain is divided into a 151×81 grid system and the time step used is 0.01 μs after many preliminary calculations with different grid size and time step.

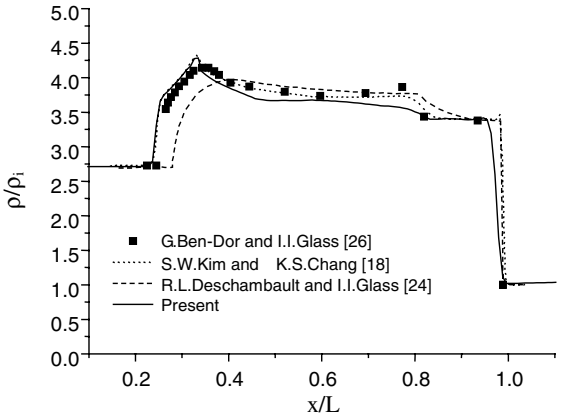

Fig. 2. Non-dimensional density distribution along the wall ($\theta_w = 27°$, $M_s = 2.03$, $T_\infty = 299.2$ K, $P_\infty = 33325$ Pa) [18,24,26].

5. Results and discussion

Now, the effects of the dust suspension on the flow are examined in the below by changing the particle parameters such as particle mass density and particle specific heat. Reacting as well as non-reacting particles are considered in this study for the operating conditions listed in Table 1.

Before the numerical results are discussed, the computational techniques used are validated by comparison with the following two cases: (1) inviscid flow along a 27.0° ramp [24] and (2) inert particle-laden gas flow in a duct [2]. In the former case, a 151×81 grid system was used to find the numerical solution. The moving shock wave of $M_s = 2.03$ enters the inlet at the initial state and the calorically perfect air is assumed. Fig. 2 presents the non-dimensional density distribution along the wall. The current result was found to be in good agreement with experimental and numerical data except for that there is a little deviation from experimental data along the ramp corner to the slipline starting point. But in overall it is better than that of Deschambault and Glass [24]. The result by S.W. Kim and K.S. Chang fits better than the present result in comparison with the experimental data, but the present result also shows the same detailed shock structure as done by S.W. Kim and K.S. Chang, for example, the compression corner, the slip line, the position of shock wave front and so on. Consequently the developed code here can still be applied to the present study. In the latter case, a 151×51 grid system was set up to simulate the two-dimensional duct. To obtain the one-dimensional inert particle-laden gas flow result from two-dimensional one, the output data at duct centerline were used. Fig. 3 illustrates the variations of the gas temperature, velocity and pressure, and the particle temperature and velocity behind a shock wave for 10 μm glass spheres suspended in air for a mass flow ratio $\eta = 0.2$, a particle–gas specific heat ratio $\delta = 1.125$ and a shock Mach number $M_s = 1.70$. Especially, the drag coefficient and the Nusselt number employed in this case are based on Ingebo's drag coefficient and the steady flow correlation for the Nusselt number. The reason is that the numerical results would be significantly affected by the corresponding models used in calculation [2]. All of the physical variables except pressure match well with Rudinger's one-dimensional numerical results.

Based on these validations, in the following the results obtained with the current code developed here would be presented and discussed for various cases.

Table 1
Operating conditions for particle-laden gas flow

	Without reaction	With reaction
Working fluid	Air	Oxygen
Gas temperature (K)	299.2	800
Gas pressure (Pa)	33325	33325
Mach number	2.03	2.03
Angle (°)	27	27
Particle diameter (μm)	1	1
Particle mass fraction	0.23	0.23
Particle mass density (kg/m^3)	3000–8000	2248.2
Particle specific heat (J/kg K)	1380–5520	Third order polynomial

5.1. Pure gas

In order to understand the transient structure of shock wave, its interaction with the pure gas (oxygen) is

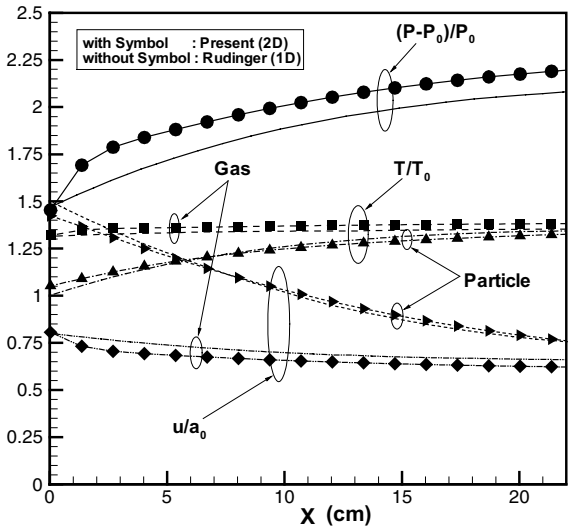

Fig. 3. Comparison of the gas temperature, velocity, and pressure, and particle temperature and particle velocity behind a shock wave for 10 μm glass spheres suspended in air for a mass–flow ratio $\eta = 0.2$, $\delta = 1.125$, and a shock Mach number.

considered prior to two-phase analysis. The transient gas density contours are plotted in Fig. 4, which clearly shows the shock wave, contact discontinuity and reflected shock wave.

At the region before the incident shock reaches, its physical properties are the same as those of the initial state. After it arrives at the ramp corner, the reflected shock wave is formed and expanding out of the corner. As time passes, the incident shock moves along the slope and simultaneously, the reflected shock region as well as the Mach step grows. The density contour at $t = 50$ μs is magnified and redrawn in Fig. 5 to show its detailed structure. The slip line, i.e., a weak discontinuity, that separates the thermodynamic regions of different density, is denoted therein together with Mach stem and triple point at which the incident shock, the reflected shock and the Mach stem encounter each other.

5.2. Non-reacting particle-laden gas

Now, in this section the non-reacting particle-laden gas is examined when it is hit by the incident shock wave. Before discussing its interaction and physical development, the velocity and temperature relaxation times are calculated as in [25] in order to assess the rate of interaction between gas and particles. When the particle diameter, density and specific heat are 1 μm, 4000 kg/m^3 and 1380 J/kg K respectively, it becomes

$$\tau_v = \frac{\sigma_p D_p^2}{18\mu} = 12.35 \times 10^{-6} = 12.35\ \mu s, \tag{23}$$

$$\tau_T = \frac{3}{2} Pr\delta\tau_v = 19.07 \times 10^{-6} = 19.07\ \mu s, \tag{24}$$

where δ is the ratio of the particle specific heat to the gas specific heat. The temperature relaxation time is nearly one and half times longer than that of velocity so that it takes about as much longer for the particle temperature to reach the gas temperature than for the particle velocity to reach the gas velocity. Therefore, there is a more possibility for thermal non-equilibrium than for dynamic non-equilibrium between particle and gas phases.

In the below, especially the effects of particle density and particle specific heat on the transient development of thermo-fluid mechanical characteristics are discussed.

5.2.1. Effects of particle mass density

As seen in Fig. 1, an incident shock wave of the Mach number M_s is propagating from left to right hand side toward a compressive corner where a two-phase medium exists. When the medium is hit by the shock wave, a transient thermo-fluid mechanical characteristic is to be developed thereafter.

Variations of the gas density, particle concentration, gas temperature and Mach number are represented in Fig. 6 for two particle mass densities of 3000 and 8000 kg/m^3. It must be noted that the particle mass fraction and its size is fixed here so that the particle number density decreases when the particle mass density increases. Furthermore, when the particle mass density is varied, the velocity as well as temperature relaxation time is also changed according to Eqs. (23) and (24). Table 2 lists their variations when the particle specific heat $C_{pp} = 1380$ J/kg K is kept constant. It reveals that as the particle mass density increases, so does each relaxation time. It means that more time is required from gas to accelerate and heat up the particles.

Fig. 6(a) reveals that as the particle mass density decreases, particles move farther upstream along the ramp and are getting denser. This is more obviously manifested in Fig. 7(a). Simultaneously, as shown in Fig. 7(b) the gas density also becomes higher with decreasing the particle mass density, since a more gas momentum is transferred to the particles so that the gas more decelerates. This can be also more clearly figured out in Fig. 7(b). This figure also shows that the shock wave speed is the slowest for the lower particle mass density. When the particle mass density is higher, there is a less momentum interaction between gas and particles after the shock wave, since the particle number density is lower. This leads to the fact that the gas velocity slowly decreases, while the particle velocity gradually increases for the case of particle mass density of 8000 kg/m^3 as in Fig. 8(a). The same reasoning applies to the thermal interaction. This results in that the gas temperature slowly

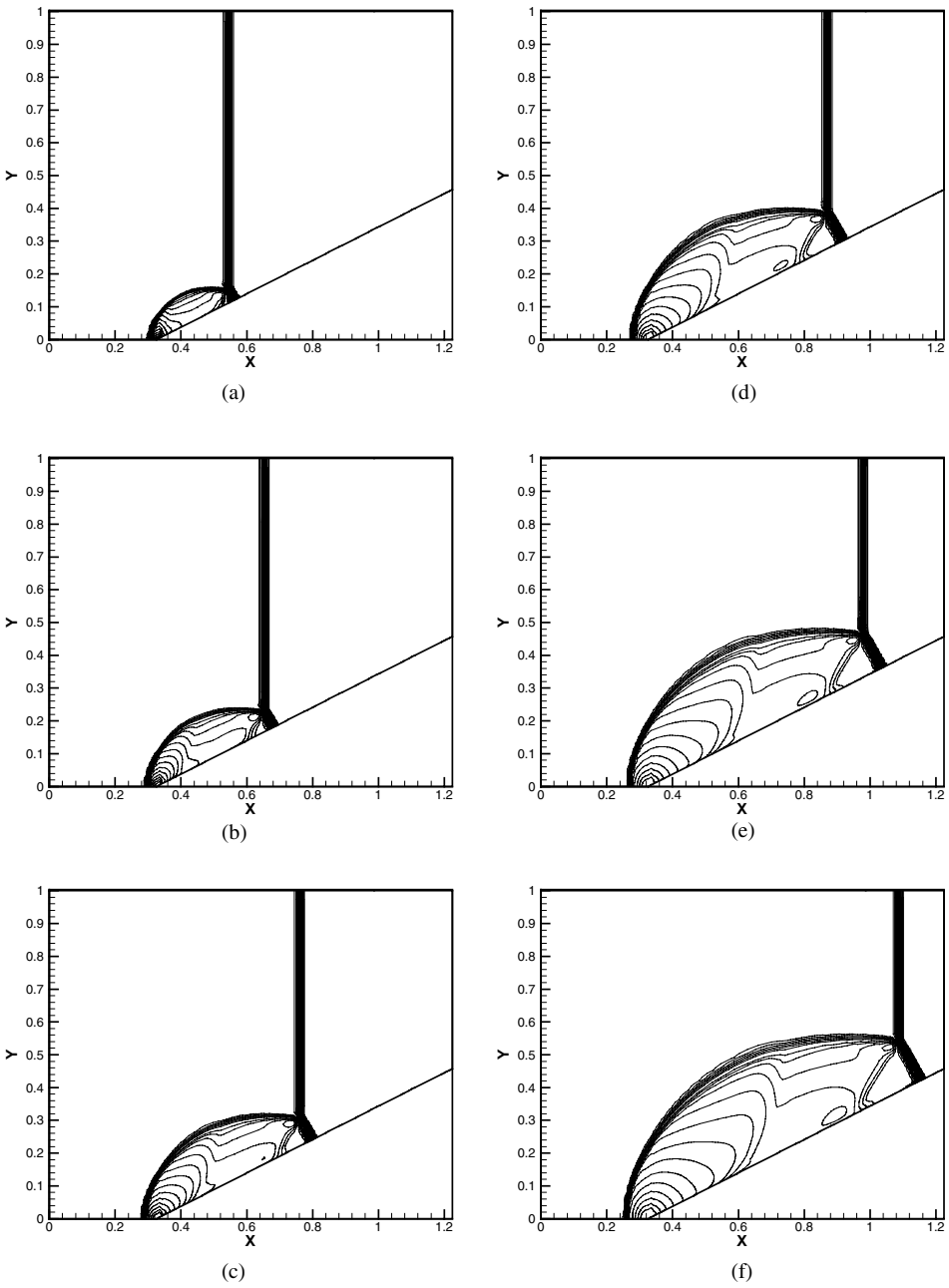

Fig. 4. Transient development of density contour for pure oxygen: (a) $t = 25$ μs, (b) $t = 30$ μs, (c) $t = 35$ μs, (d) $t = 40$ μs, (e) $t = 45$ μs, (f) $t = 50$ μs.

decreases, while the particle temperature slowly increases for the case of particle mass density of 8000 kg/m^3 as in Fig. 8(b). Consequently, for the case of particle mass density of 8000 kg/m^3, a longer distance is required for the thermal equilibrium to be attained after the shock wave. Overall distributions of gas temperature and Mach number are plotted in Fig. 6(c) and (d) in which their variations behind the shock wave are sluggish for the higher particle mass density.

5.2.2. Effects of particle specific heat

A change in the particle specific heat would also change the velocity and temperature relaxation times as

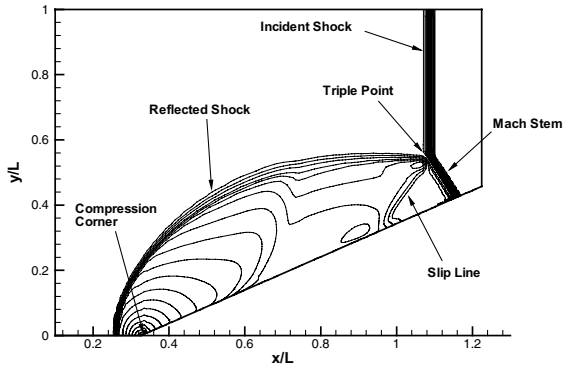

Fig. 5. Detailed structure of density contour for pure oxygen at $t = 50$ μs.

shown in Table 2. When the particle mass density $\rho_p = 4000$ kg/m^3 is kept constant, the velocity relaxation time is not changed, while the temperature relaxation time increases with an increase in the particle specific heat.

Since the velocity relaxation time is constant, one may think that the variation of the particle specific heat would not influence the particle concentration field as in Fig. 9(a). However, the particle concentration distribution is affected by gas velocity through momentum transfer between gas and particles. Since the gas velocity is directly influenced by the gas density that depends on the gas temperature, the change in particle specific heat indirectly affects the particle concentration as shown in its detailed variation in Fig. 10(a). But, there is a direct effect of the particle specific heat on the gas as well as particle temperature variation as in Fig. 9(c) and (d). As the particle specific heat increases, there exists a strong thermal interaction between gas and particles due to a big temperature difference between two phases so that the gas temperature quite rapidly decreases after the shock wave while the particle temperature very slowly increases due to its higher particle specific heat as illustrated in Fig. 11(a). That is why the gas density becomes higher as the particle specific heat is higher as in Fig. 10(b), while its two-dimensional variation is plotted in Fig. 9(b). Fig. 9(e) represents a variation of Mach number due to particle specific heat. Only a minor effect is observed.

In Fig. 11(b), a variation of gas and particle velocity with particle specific heat is drawn. Due to its indirect influence, only a small reduction in gas as well as particle velocity is noted for the case of higher particle specific heat.

Here, the effects of particle diameter and particle loading are only to be briefly discussed since they are usually common. When either the particle size is smaller or the particle loading is higher, the speed of shock wave propagation becomes slower. The reason is that the momentum exchange between gas and particles becomes more active so that the gas momentum is easily transferred to the particles. By the same reason, the thermal exchange between gas and particles is more enhanced so that the temperature difference between two phases is also reduced.

5.3. Reacting particle-laden gas

When the carbon particles are reacting in the high temperature environment caused by the shock wave (greater than 1000 K), the thermal properties are expected to be more changeable. However, the dynamic phenomena are only indirectly affected by the particle reaction through heat transfer to gas phase, as shown in Fig. 12. Therefore, only a minor change is observed in the particle concentration distribution (Fig. 12(a)) and the Mach number distribution (Fig. 12(d)), while the gas density and temperature contours (Fig. 12(b) and (c)) show a more obvious change in the relaxation zone when the chemical reaction occurs.

The gas density and pressure distribution along the wall are plotted in Fig. 13. The case for pure gas is definitely distinguished from the cases with inert or reacting particles. For the case with particles the shock wave propagates slower and the variation of gaseous density and pressure is more variable in the relaxation zone due to the active interaction of gas and particles regardless of the chemical reaction. Just behind the Mach stem regime where the shock front is located, the gaseous density for the case with particles is even higher than that for the pure gas case, since the gas velocity is reduced due to momentum interaction between gas and particles. However, in the relaxation zone the gaseous density with inert particles further increases, while the gaseous density for the reacting case abruptly decreases due to the intense thermal interaction and chemical reaction. But, at the compression corner, all the gaseous densities become the same, for the particles no longer exist there. According to Fig. 13(b), the pressure for pure gas is lower than that with particles after the shock wave, since there is no momentum loss to the particles. The pressure for reacting particles is even higher than that for non-reacting particles, for the gas temperature becomes much higher due to chemical reaction.

The gas and particle temperature and velocity distributions along the wall are shown in Fig. 14. As could be expected, until the carbon ignition (just behind the Mach stem), identical temperature variations are obtained for the non-reacting and reacting particles. However, after the carbon starts burning, the gas and particle temperatures exceed those obtained for inert particles as seen in Fig. 14(a). Based on the gas

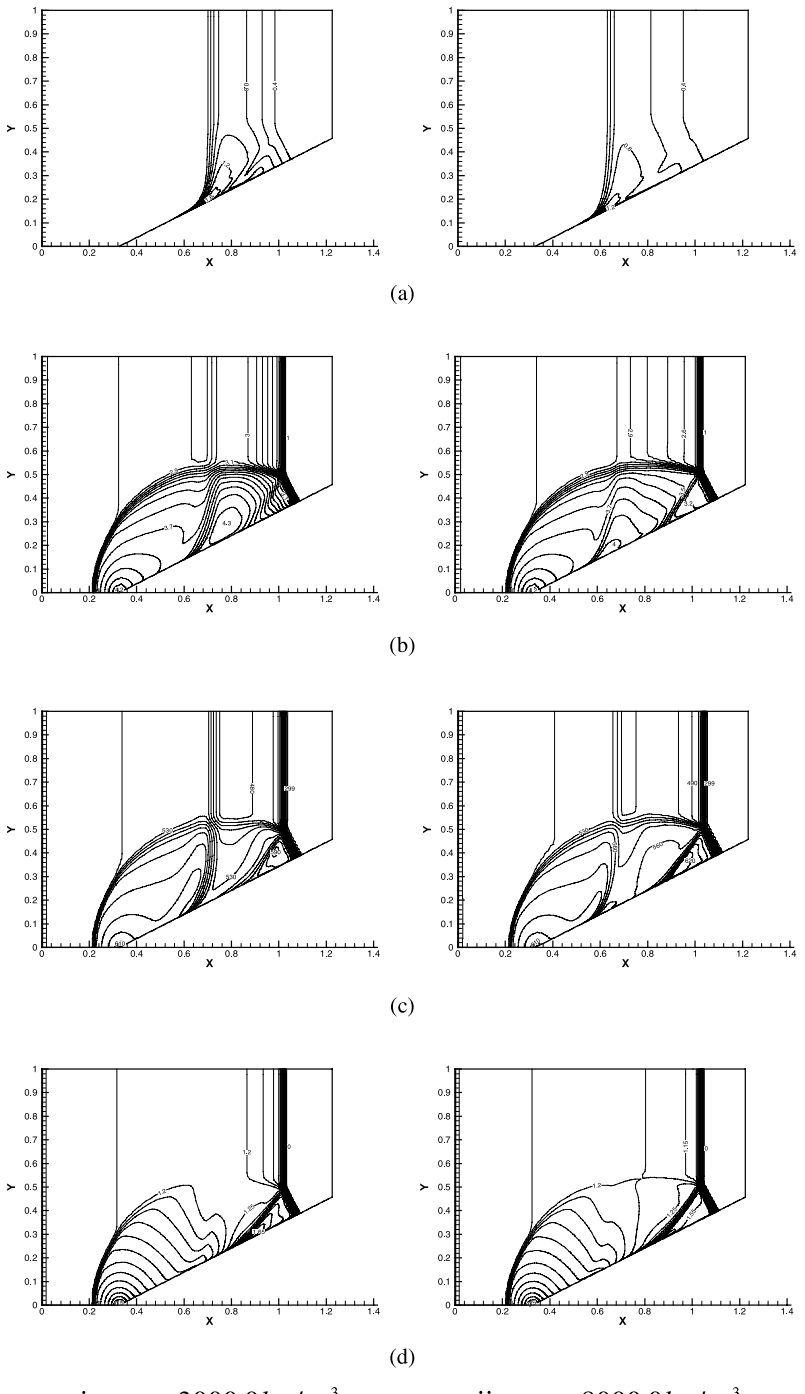

Fig. 6. Effects of particle mass density on various contours at $t = 75.8$ μs: (a) particle concentration contours; (b) gas density contours; (c) gas temperature contours; (d) Mach number contours.

temperature for pure gas case, the gas as well as particle temperature for non-reacting particles is observed to be lower due to thermal interaction between gas and particles.

Table 2
Variation of the velocity and temperature relaxation times with the particle mass density and the particle specific heat

	Particle mass density (kg/m^3)		Particle specific heat (J/kg K)	
	3000	8000	1380	5520
t_v (μs)	12.35	24.69	12.35	12.35
t_T (μs)	19.07	38.15	19.07	76.30

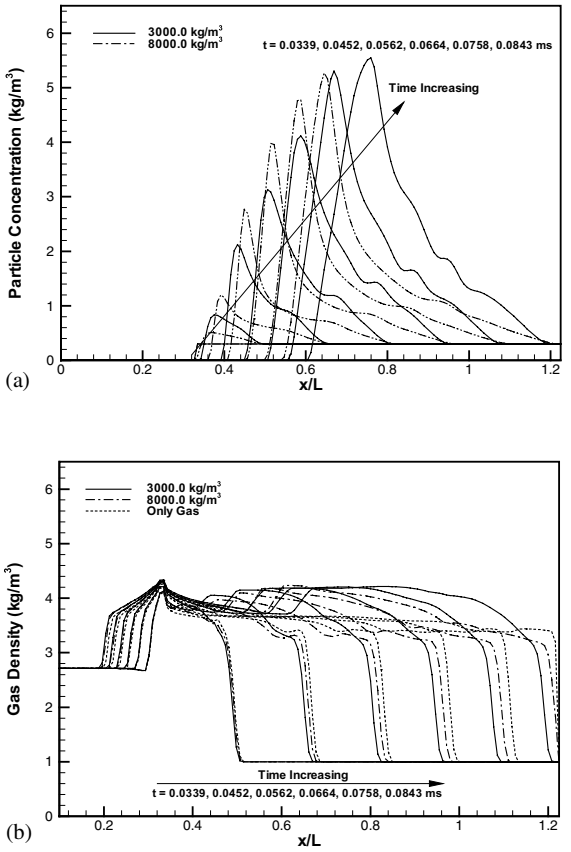

Fig. 7. Effects of particle mass density on particle concentration and gas density: (a) transient variation of particle concentration; (b) transient variation of gas density.

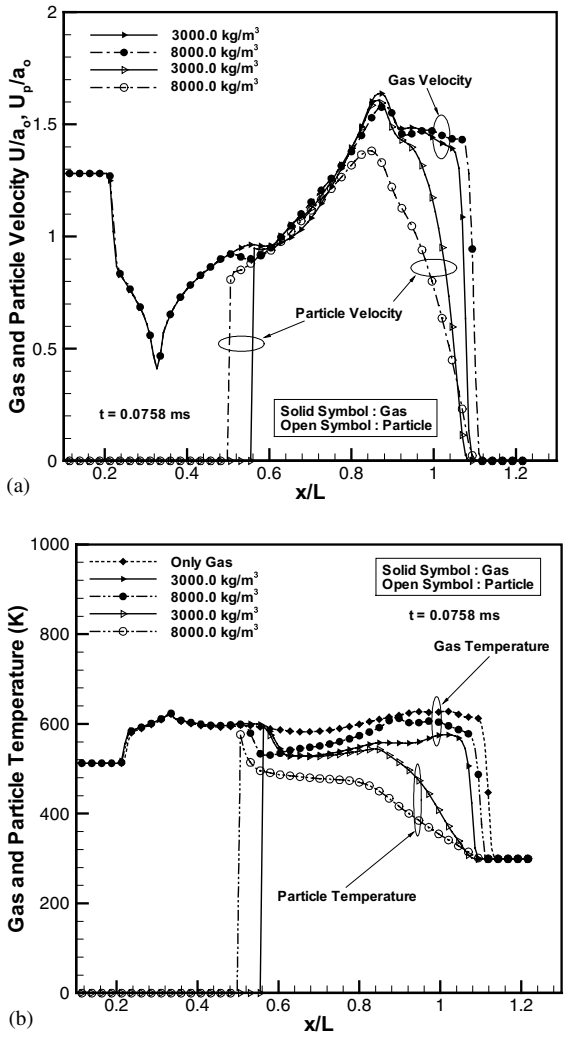

Fig. 8. Effects of particle mass density on velocity and temperature distributions along the wall at $t = 75.8$ μs: (a) gas and particle velocity distributions; (b) gas and particle temperature distributions.

As shown in Fig. 14(b), the maximum gas velocity becomes the highest for pure gas case, since there is no momentum loss to the particles. For the case with particles, the gas as well as particle velocity follows the same trend before the carbon ignition occurs, regardless of the chemical reaction. Right after the carbon ignition, however, the gas and the particle velocities exceed those for the non-reacting particles. In the relaxation zone, it is observed that the gas and particle velocities become lower for the reacting case than those for the non-reacting case. The reason is deduced from Fig. 13(b), in which the active chemical reaction induces a stronger adverse pressure gradient. Therefore, the gas velocity for reacting particles is even further reduced than the particle velocity as in Fig. 14(b).

6. Concluding remarks

The conservative equations for an analysis of a moving shock wave interaction with two-phase medium were formulated and numerically solved. Different from

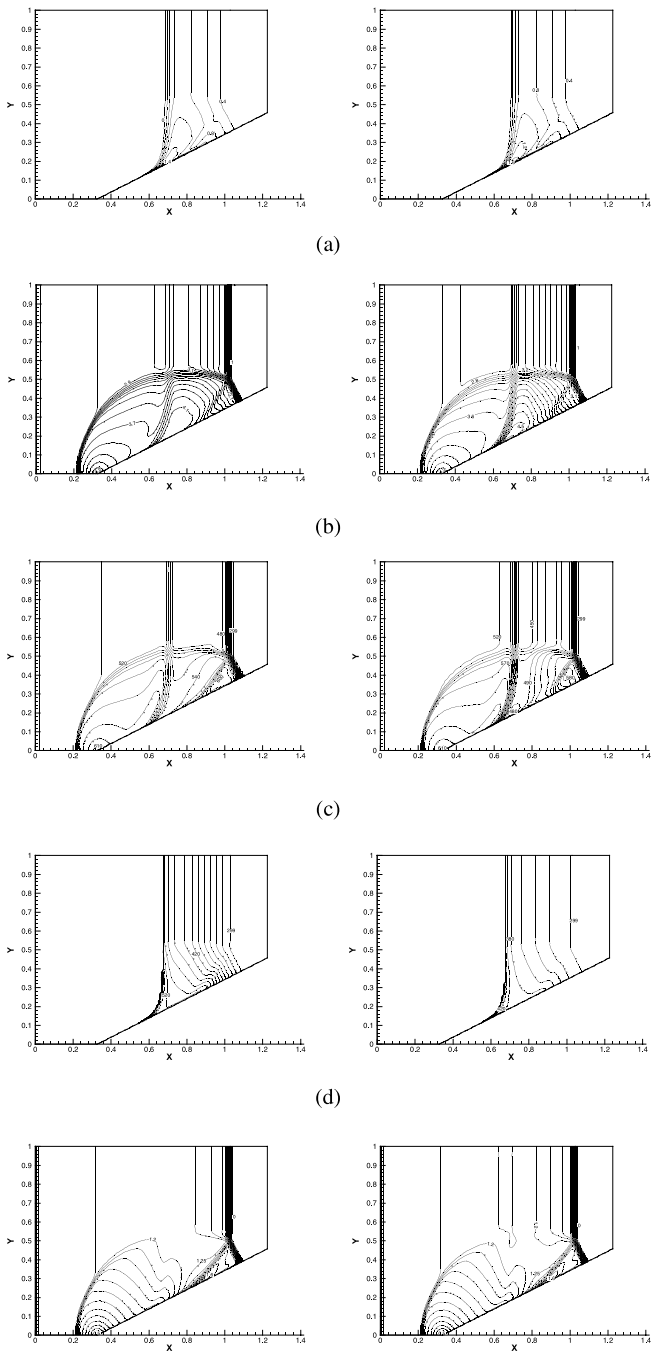

Fig. 9. Effects of particle specific heats on various contours at $t = 75.8$ μs: (a) particle concentration contours; (b) gas density contours; (c) gas temperature contours; (d) particle temperature contours; (e) Mach number contours.

the previous literatures, this paper was focused on the effects of the particle mass density and the particle specific heat on the thermo-fluid mechanical characteristics. Furthermore, the thermo-fluid mechanical developments

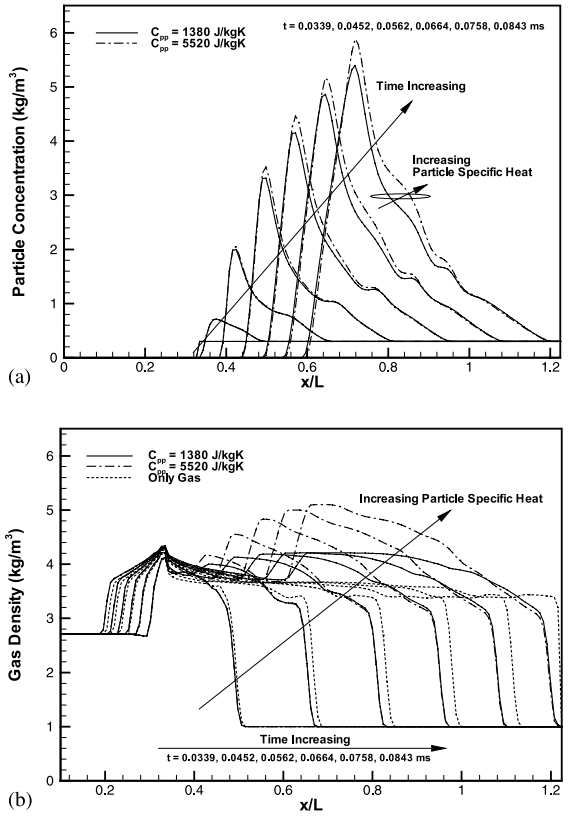

Fig. 10. Effects of particle specific heat on particle concentration and gas density: (a) transient variation of particle concentration; (b) transient variation of gas density.

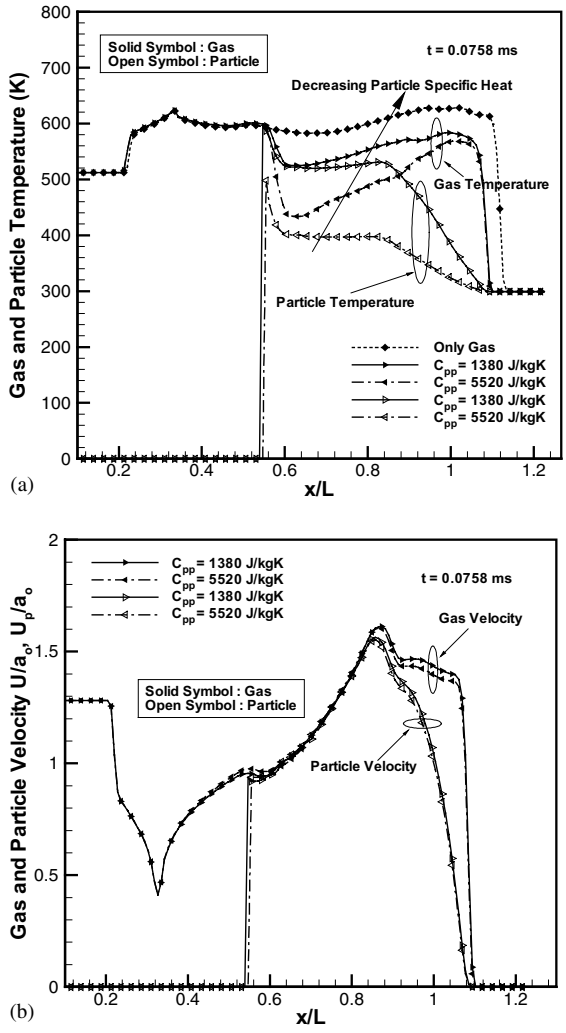

Fig. 11. Effects of particle specific heat on velocity and temperature distributions at $t = 75.8$ μs: (a) gas and particle temperature distributions; (b) gas and particle velocity distributions.

have also been examined for two-dimensional interaction with two-phase flow with reacting particles.

For the unsteady flow, the velocity as well as temperature relaxation time played an important role. When they were shorter, the interaction between gas and particles were so intense that the dynamic and thermal equilibriums were attained in a shorter time. Further results showed that

1. As the particle mass density decreases, the gas and particles more closely follow the shock front farther upstream and the particle concentration becomes denser behind the shock wave. The thermal and momentum exchange between gas and particles becomes so intense that temperature and velocity differences between gas and particles more rapidly decrease.
2. The particle specific heat exerts only an indirect effect on the particle concentration and the velocity field. However, when the particle specific heat is higher, the gas temperature rapidly decreases while the particle temperature slowly increases.
3. In the reacting particle-laden gas flow, the dynamic variation is only secondary to the thermal one.
4. For the inert particle-laden gas flow, the gas density becomes even higher than that in the pure gas flow in the relaxation zone, while for the reacting case the gas density abruptly decreases due to higher gas temperature caused by the active chemical reaction.
5. In the relaxation zone, the gas as well as particle velocity for reacting particles becomes lower than that for non-reacting particles due to a stronger adverse pressure gradient due to chemical reaction.

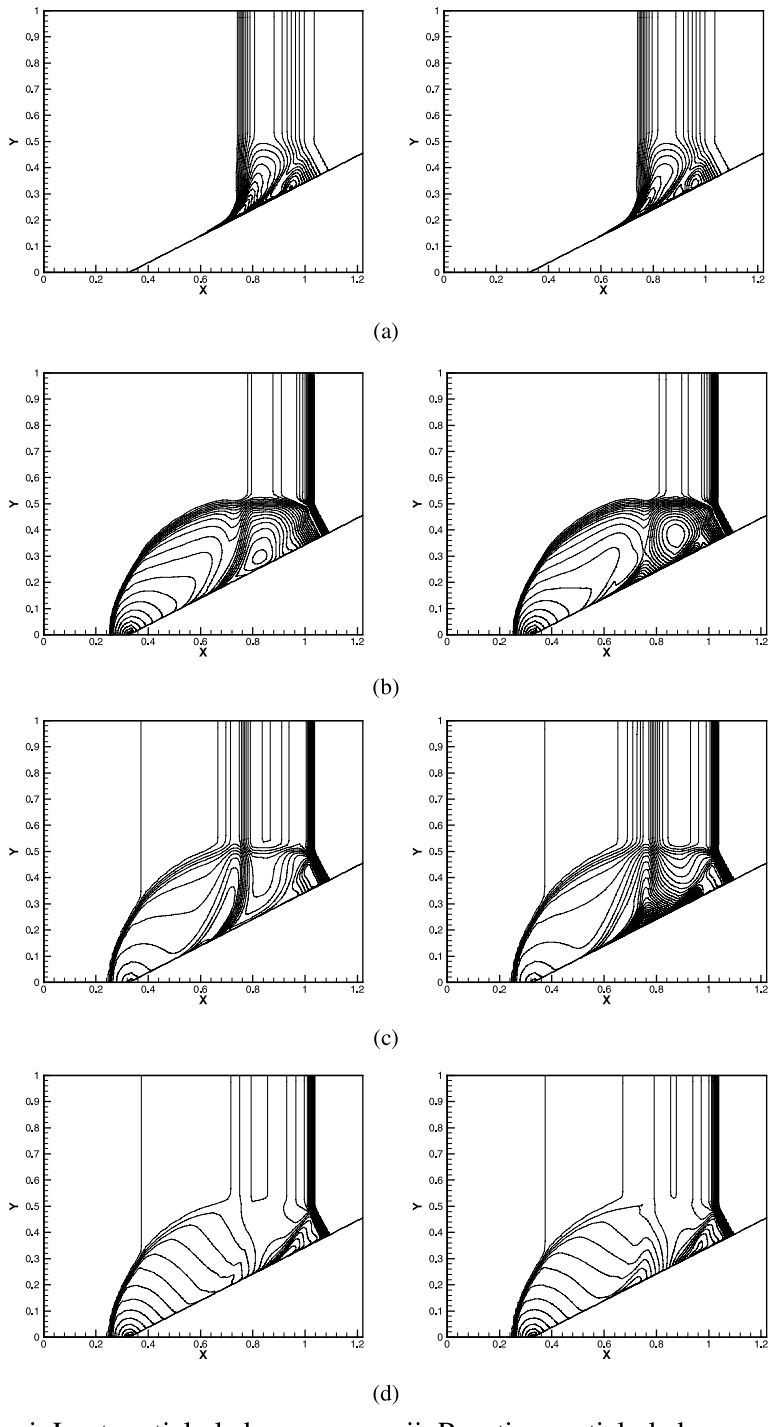

Fig. 12. Comparison of various contours for inert and reacting particle-laden gases at $t = 50$ μs: (a) particle concentration contours; (b) gas density contours; (c) gas temperature contours; (d) Mach number contours.

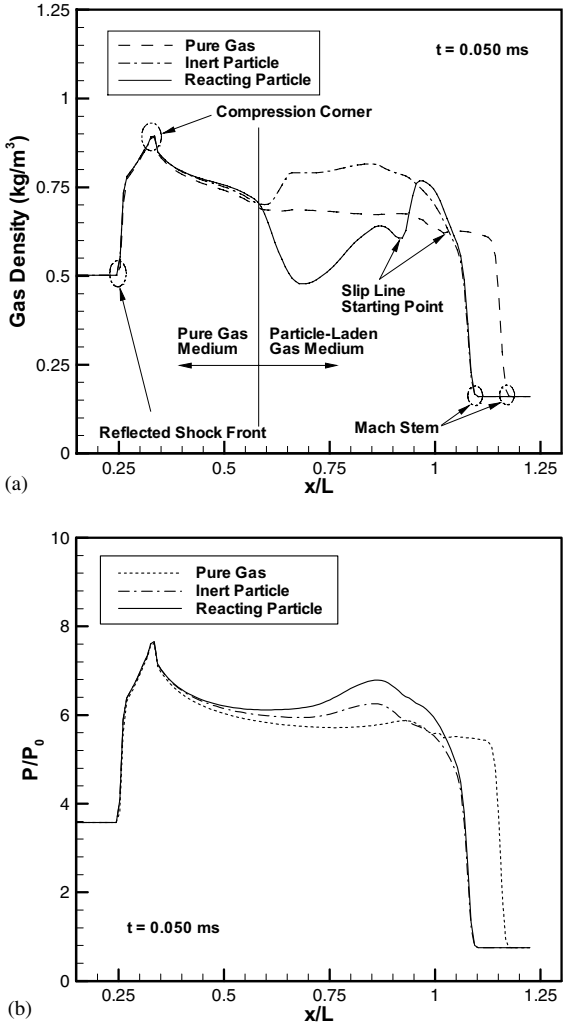

Fig. 13. Comparison of gas density and pressure distributions along the wall at $t = 50$ μs: (a) gas density distributions; (b) pressure distributions.

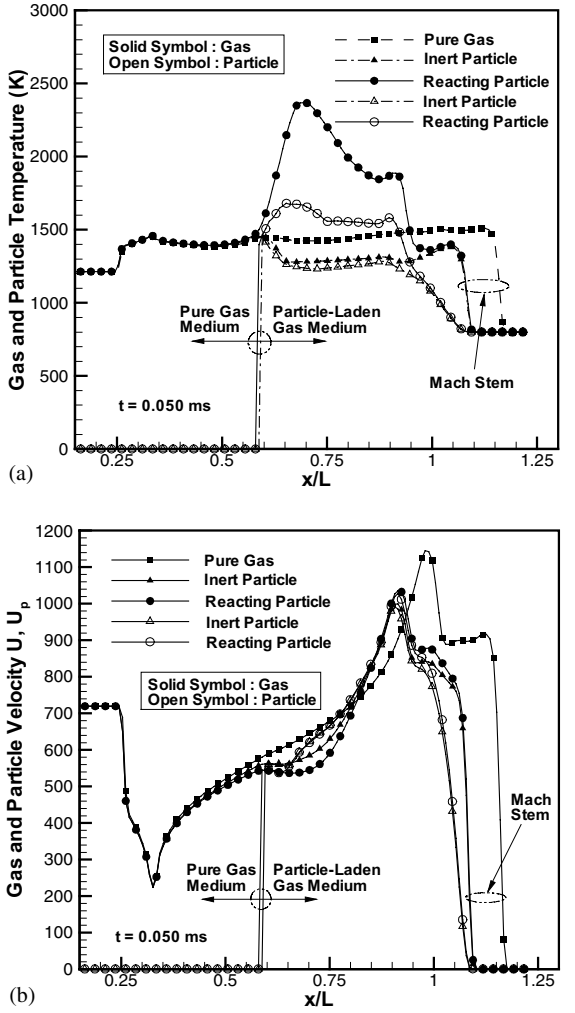

Fig. 14. Comparison of temperature and velocity distributions along the wall at $t = 50$ μs: (a) gas and particle temperature distributions; (b) gas and particle velocity distributions.

Acknowledgements

This research was supported by Agency for Defense Development, Korea, through the Center for ElectroOptics at the KAIST.

References

[1] G.F. Carrier, Shock waves in a dusty gas, J. Fluid Mech. 4 (1958) 376–382.
[2] G. Rudinger, Some properties of shock relaxation in gas flows carrying small particles, Phys. Fluids 7 (1964) 658–663.
[3] R.F. Hoglund, Recent advances in gas–particle nozzle flows, ARS J. (1962) 662–671.
[4] C.T. Crowe, Review-numerical models for dilute gas–particle flows, J. Fluids Eng. 104 (1982) 297–303.
[5] I-Shih. Chang, One- and two-phase nozzle flows, AIAA J. 18 (1980) 1455–1461.
[6] F. Marconi, S. Rudman, V. Calia, Numerical study of one-dimensional unsteady particle-laden flows with shocks, AIAA J. 19 (1981) 1294–1301.
[7] I. Elperin, O. Igra, G. Ben-Dor, Analysis of normal shock waves in a carbon particle-laden oxygen gas, J. Fluid Eng. 108 (1986) 354–359.
[8] O. Igra, G. Ben-Dor, I. Elperin, Parameters affecting the postshock wave relaxation zone in an oxygen carbon particle suspension, J. Fluid Eng. 108 (1986) 360–365.
[9] S.S. Gokhale, T.K. Bose, Reacting solid particles in one-dimensional nozzle flow, Int. J. Multiphase Flow 15 (1989) 269–278.

[10] M. Nishida, S. Ishimaru, Numerical analysis of gas–solid two-phase non-equilibrium nozzle flows, JSME Int. J. Ser. II 33 (1990) 494–500.
[11] R.C. Mehta, T. Jaychandran, A fast algorithm to solve viscous two-phase flow in an axisymmetric rocket nozzle, Int. J. Numerical Methods Fluids 26 (1998) 501–517.
[12] O. Igra, I. Elperin, G. Ben-Dor, Dusty gas flow in a converging–diverging nozzle, J. Fluids Eng. 121 (1999) 908–913.
[13] G. Bendor, O. Igra, L. Wang, Shock wave reflections in dust–gas suspensions, J. Fluids Eng. 123 (2001) 145–153.
[14] T.H. Pulliam, Time accuracy and the use of implicit methods, AIAA Paper 93-3360, AIAA 11th Computational Fluid Dynamics Conference, Orlando, FL, 1993.
[15] H.C. Yee, Construction of explicit and implicit symmetric TVD schemes and their applications, J. Comput. Phys. 68 (1987) 151–179.
[16] H.C. Yee, A class of high resolution explicit and implicit shock-capturing methods, NASA TM-101099, 1989.
[17] R. Saurel, E. Daniel, J.C. Loraud, Two-phase flows: second-order schemes and boundary conditions, AIAA J. 32 (1994) 1214–1221.
[18] S.W. Kim, K.S. Chang, Reflection of shock wave from a compression corner in a particle-laden gas region, Shock Waves 1 (1991) 65–73.
[19] R. Cliff, J.R. Grace, M.E. Weber, Bubbles, Drops and Particles, Academic Press, New York, 1978.
[20] C.B. Henderson, Drag coefficients of spheres in continuum and rarefied flows, AIAA J. 14 (1976) 707–708.
[21] D.J. Carlson, R.F. Hoglund, Particle drag and heat transfer in rocket nozzles, AIAA J. 2 (1964) 1980–1984.
[22] S.W. Baek, S.P. Seung, Parametric analysis on the post-shock wave relaxation zone of carbon particle-laden oxygen gas, Combust. Flame 80 (1990) 126–134.
[23] A. Jameson, E. Turkel, Implicit schemes and LU decompositions, Math. Comput. 37 (1981) 385–397.
[24] R.L. Deschambault, I.I. Glass, An update on non-stationary experiments, J. Fluid Eng. 14 (1983) 27–57.
[25] G. Rudinger, Fundamentals of Gas–Particle Flow, Elsevier Scientific Publishing Company, 1980.
[26] G. Bendor, I.I. Glass, Domains and boundaries of non-stationary oblique shock wave reflections. 1. Diatomic gas, J. Fluid Mech. 92 (1979) 459–496.